Long range spin ferromagnetic order with zero magnetization in (111)$Sm_{1-x}Gd_xAl_2$ films

2008 J. Phys.: Condens. Matter 20 265001

(http://iopscience.iop.org/0953-8984/20/26/265001)

J. Phys.: Condens. Matter **20** (2008) 265001 (8pp) doi:10.1088/0953-8984/20/26/265001

Long range spin ferromagnetic order with zero magnetization in (111)$Sm_{1-x}Gd_xAl_2$ films

A Avisou[1], C Dufour[1], K Dumesnil[1], A Rogalev[2], F Wilhelm[2] and E Snoeck[3]

[1] Laboratoire de Physique des Matériaux, Université H Poincaré Nancy I, BP 239, 54506 Vandoeuvre les Nancy cédex, France
[2] European Synchrotron Radiation Facility, 6 rue Jules Horowitz, BP 220, 38043 Grenoble, France
[3] CEMES BP 94347, 31055 Toulouse cedex 4, France

Received 22 January 2008, in final form 13 April 2008
Published 22 May 2008
Online at stacks.iop.org/JPhysCM/20/265001

Abstract

Bulk $Sm_{1-x}Gd_xAl_2$ ($0.01 < x < 0.035$) compound exhibits an exciting magnetic property: its magnetization drops to zero at a compensation temperature T_{comp} while it maintains a long range ferromagnetic order. We achieved recently the first epitaxial growth of (111)$Sm_{1-x}Gd_xAl_2$ films by molecular beam epitaxy. Macroscopic magnetization measurements confirmed the existence of a magnetic compensated state, occurring at a temperature that depends on the concentration of Gd. Specific features observed in the $Sm_{1-x}Gd_xAl_2$ films are a strong [111] perpendicular anisotropy and a very large coercivity. X-ray magnetic circular dichroism at Sm and Gd $L_{2,3}$ edges allows us to directly evidence the existence of a long range magnetic polarization of the Sm and Gd sublattices at T_{comp}, and a parallel coupling between the total magnetic moment of Sm^{3+} and Gd^{3+}. Moreover, it is possible to tailor the magnetic behavior at T_{comp} by changing the thermo-magnetic treatment.

1. Introduction

The ferromagnetic Sm intermetallic compound $SmAl_2$ has attracted much attention because of the unique magnetic properties of the Sm^{3+} ion [1]. As an element of the first half of the rare earth series, Sm 4f spin and orbital moments are antiparallel coupled by the spin–orbit interaction. Moreover, their close magnitudes give rise to a very small net 4f magnetic moment dominated at every temperature by the orbital component. As a result, the contributions from conduction electrons and doping ions to the net magnetic moment become important. Adachi *et al* [2] created a compensated system by substituting Sm with Gd to form $Sm_{1-x}Gd_xAl_2$. These compounds present a compensation temperature T_{comp} at which a long range ferromagnetic order persists while the net magnetization is zero [2]. This temperature depends on the Gd concentration. At T_{comp}, the total spin and orbital moments, including the contributions from Gd ions and conduction electrons, canceled out. Gd^{3+} ions with a half-filled 4f orbital present only a spin contribution to the magnetic moment (the orbital moment being zero), leading to the canceling at T_{comp} of the Sm^{3+} orbital magnetic moment excess. The existence of ferromagnetic order at T_{comp} was proven on bulk $Sm_{1-x}Gd_xAl_2$ through several experiments [3–5]. In particular, magnetic Compton scattering [4] proved the existence of ferromagnetic ordering of the conduction electron spin at T_{comp}; x-ray magnetic circular dichroism (XMCD) at the Sm^{3+} and Gd^{3+} $M_{4,5}$ edges [5] attested to long range order of the 4f spin and orbital moments.

These zero-moment ferromagnets are of considerable interest in the field of devices processing the spin of charged particles, for example in spin-polarized STM and spintronics devices, as pointed out by Qiao *et al* [6]. They present the advantage that they do not generate any disturbing magnetic field, and are not sensitive to an external field. Therefore, the next step is the elaboration of $Sm_{1-x}Gd_xAl_2$ epitaxial films and the study of their magnetic properties.

This paper reports on the first results obtained for single crystalline (111)$Sm_{1-x}Gd_xAl_2$ films. Section 2 is devoted to film fabrication using molecular beam epitaxy and to structural characterization. The anisotropy, coercivity and compensation state in (111)$Sm_{1-x}Gd_xAl_2$ films are presented in section 3,

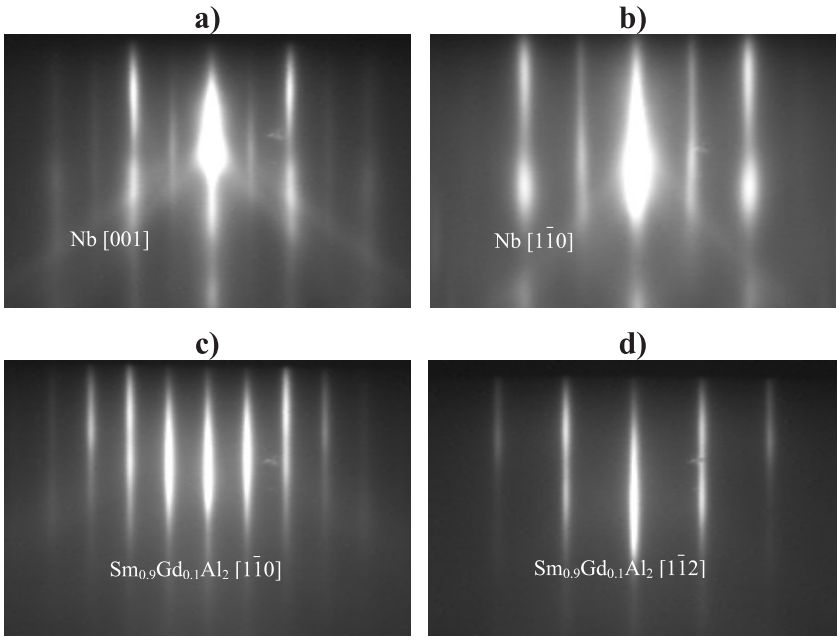

Figure 1. RHEED patterns collected at 510 °C along Nb [001] and Nb [1$\bar{1}$0] azimuth directions, and along [1$\bar{1}$0]$Sm_{0.9}Gd_{0.1}Al_2$ and [11$\bar{2}$]$Sm_{0.9}Gd_{0.1}Al_2$ azimuth directions.

in comparison with pure $SmAl_2$ films without Gd substitution. In section 4, XMCD is shown to be a powerful technique to probe the Sm and Gd spin moment and to give a proof for the ferromagnetic order at compensation in the films, despite the zero magnetization.

2. $Sm_{1-x}Gd_xAl_2$ film fabrication and structural characterization

$SmAl_2$ belongs to the group of cubic Laves phases ($Fd\bar{3}m$) with a lattice constant of 7.943 Å at room temperature [7]. The samples were prepared by molecular beam epitaxy. Using our knowledge of the epitaxy of Laves phases [8], the growth of single crystal $Sm_{1-x}Gd_xAl_2$ films was achieved by co-deposition of samarium, gadolinium and aluminum atoms on a (110) niobium buffer, covering a (11$\bar{2}$0) sapphire substrate [9]. The deposition rates were measured by an optical sensor when the material is evaporated from electron guns (Al and Gd) and by a quartz microbalance, previously calibrated at the substrate position, when the material is evaporated from an effusion cell (Sm). Before the deposition, the Sm, Gd and Al beam fluxes are calibrated to get the target stoichiometry at the substrate position (the Gd concentration x varies between 0.01 and 0.23). The films were grown at 510 °C in order to have a (111) growth [9]. The deposition rate is 3.6 nm min^{-1} for the Laves phase compounds. The thickness of the films considered in this study varies between 88 and 880 nm. The samples were finally coated with a 50 nm thick Nb layer to prevent oxidation.

Figure 1 presents the RHEED patterns collected along the main azimuths of the 80 nm Nb buffer layer ((a) and (b)) and along the corresponding azimuths for the $Sm_{0.9}Gd_{0.1}Al_2$ deposit ((c) and (d)). For this deposition temperature, the relative orientation between the (110)Nb buffer and the (111) film is of Nishiyama–Wassermann type, with the Nb buffer and $Sm_{0.9}Gd_{0.1}Al_2$ film dense directions parallel to each other. The in-plane epitaxial relationships are [11$\bar{2}$]$Sm_{0.9}Gd_{0.1}Al_2$ ∥ [1$\bar{1}$0]Nb and [1$\bar{1}$0]$Sm_{0.9}Gd_{0.1}Al_2$ ∥ [001]Nb. The matching observed for these relative orientations (11Nb:7$Sm_{1-x}Gd_xAl_2$ along [001]Nb and 3Nb:2$Sm_{1-x}Gd_xAl_2$ along [1$\bar{1}$0] Nb) result in a −2.2% mismatch along the [001]Nb direction, and a −4.3% mismatch along the [1$\bar{1}$0] Nb direction [9].

The determination of the Gd content is difficult when using classical techniques in the range 0%–3.5% (for example, the errors are ±2% when using microprobe analysis). Thus, the Gd content is obtained from the value of the low temperature magnetization in a 7 T field.

X-ray diffraction analyses attest to the high crystalline quality of the films with a coherence length ranging between 45 and 55 ± 0.5 nm along the growth direction, and a mosaicity between 0.35° and 0.5°.

A cross-sectional transmission electron micrograph is presented in figure 2(a) for an $x = 0$ sample. The sample is studied along the [11$\bar{2}$] zone axis. The image confirms the high structural quality of the film. However, it shows the appearance of an interface phase of about 0.5 nm thick at the interface between Nb and $SmAl_2$ and the presence of an antiphase boundary (APB). This structural defect corresponds to a stacking fault between two parts of a single crystal. It may come from the growth of two different (111) planes on two areas of the substrate that results in the appearance of such APBs when the regions coalesce. The stacking defect is clearly visible on the Fourier filtered image presented in figure 2(b).

3. Anisotropy, coercivity and compensation state

The magnetic behavior in the epitaxial films has been investigated by magnetization measurements, using a Quantum

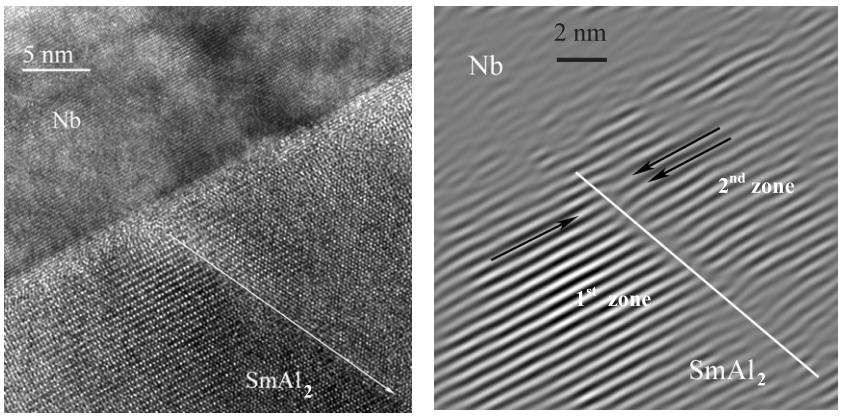

Figure 2. (a) HRTEM micrograph of a 690 nm thick (111)$SmAl_2$ film deposited on a (110)Nb buffer; (b) filtered and magnified image.

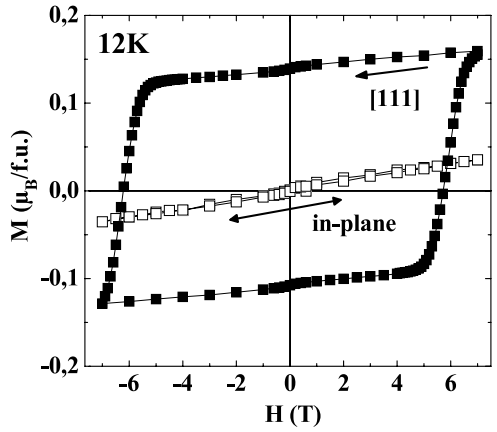

Figure 3. Hysteresis loops measured at 12 K for a 880 nm thick $Sm_{0.987}Gd_{0.013}Al_2$ film with the field applied in the growth plane (open squares) and perpendicular to the growth plane (filled squares). The sample has been cooled under a 7 T magnetic field ($H_{fc} = 7$ T).

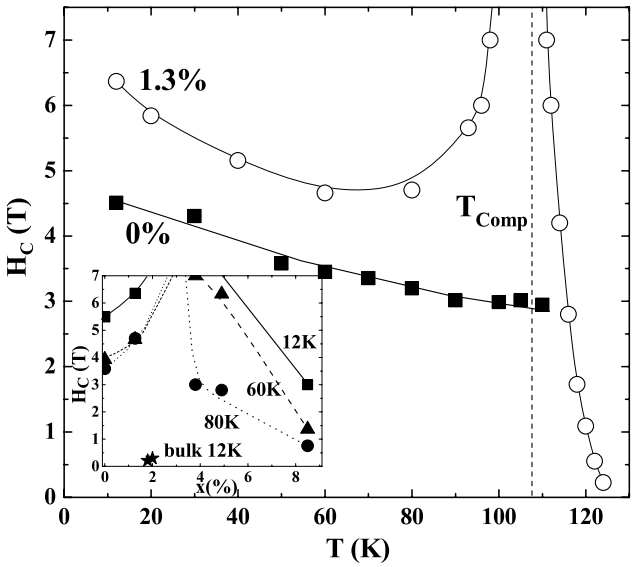

Figure 4. Temperature dependence of the coercive field for the 880 nm thick $Sm_{0.987}Gd_{0.013}Al_2$ film (circles) and for the pure $SmAl_2$ film (squares). Inset: coercive field as a function of Gd content x at 12 K (squares), at 60 K (triangles) and at 80 K (circles) and for bulk compound at 12 K (stars). The lines are guides to the eyes.

Design SQUID magnetometer. The diamagnetic contribution of the substrate has been systematically subtracted.

First, we should underline that the films exhibit a strong perpendicular anisotropy, as shown in figure 3 for a 880 nm thick film with a Gd content around 1.3%. The hysteresis loop measured at 12 K with the applied field parallel to the [111] growth direction is almost square, while the loops measured with the field applied along in-plane directions are characteristic of a magnetic hard direction. Consequently, at 12 K, the film presents an uniaxial anisotropy with an easy direction perpendicular to the growth plane. Such a uniaxial anisotropy is maintained when increasing temperature.

The [111] growth direction corresponds to one of the bulk ⟨111⟩ easy magnetization axes [10]; however, complementary experiments performed for another growth direction or another substrate have shown that the perpendicular magnetization in the films is not related to the bulk anisotropy but to the compressive strains along the growth direction [11, 12]. The lattice strain induces an enhancement of the magnetoelastic contribution to the total energy. When both the strain along the growth direction and the magnetoelastic constant b_2 are negative (as in $SmFe_2$, $ErFe_2$ [12] and $SmAl_2$ [11]), the magnetization direction shifts along the growth direction.

When changing the Gd content from 0% to 8.5%, the easy direction remains perpendicular. However, for larger Gd concentrations, the in-plane direction becomes less hard because of (i) the increase of the demagnetizing field contribution (due to the increase of the total net magnetic moment) and (ii) the small value of b_2 of Gd (correlated to the lack of orbital moment in Gd ions).

Finally, the direction of the magnetic anisotropy does not depend on the film thickness when it varies from 88 to 880 nm.

Another remarkable point is the very high coercive field measured in the perpendicular direction, reaching 6.2 T at 12 K in this 880 nm film. The observed positive vertical shift of the hysteresis loop is explained by the high coercive field which

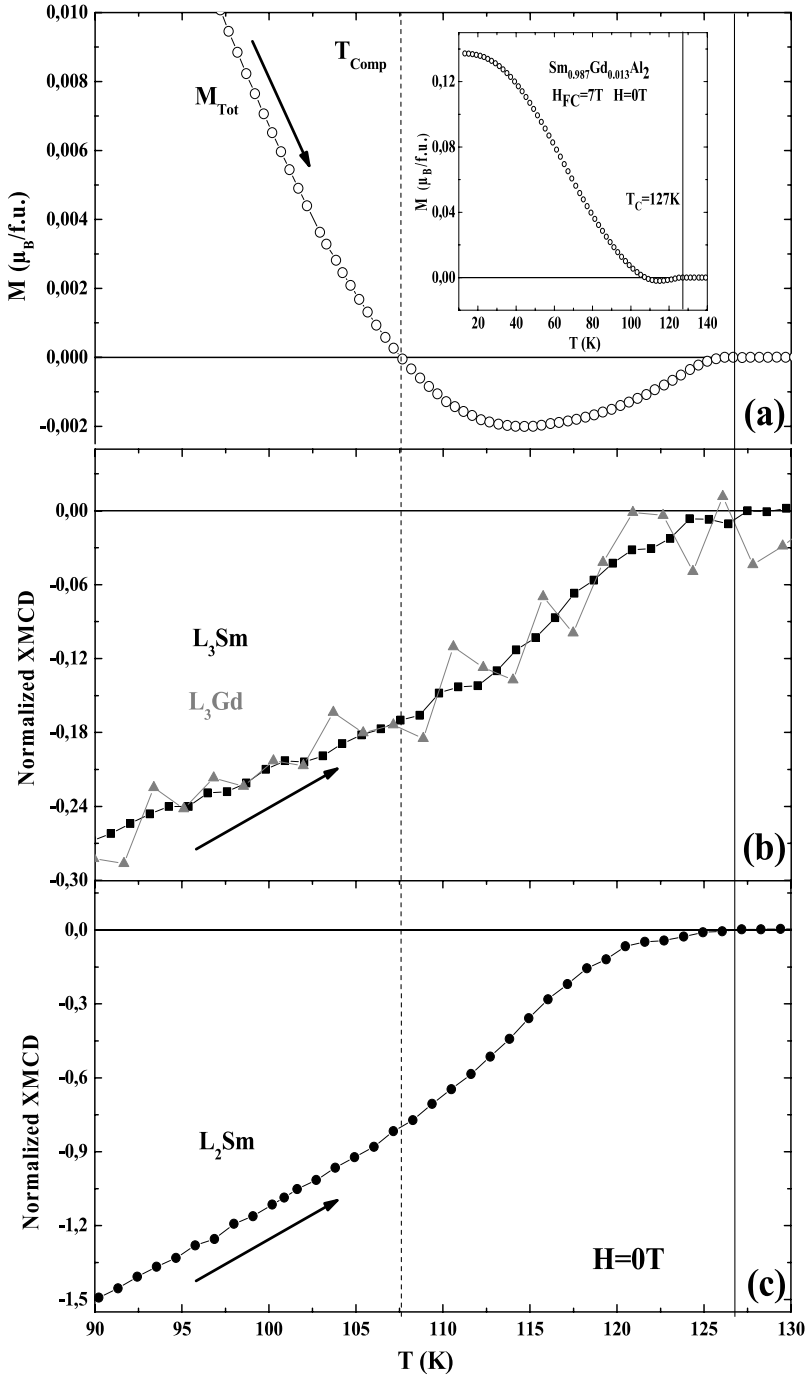

Figure 5. (a) Magnetization versus temperature measured in increasing temperature under zero magnetic field after a 7 T field cooling process for the 880 nm thick $Sm_{0.987}Gd_{0.013}Al_2$ film (the inset shows the whole temperature range). (b) XMCD signal at the Sm and Gd L_3 edge for the 880 nm thick $Sm_{0.987}Gd_{0.013}Al_2$ film. X-ray energies are respectively 6.705 and 7.246 keV. The L_3Gd signal has been multiplied by 6. (c) XMCD signal at the Sm L_2 edge for the 880 nm thick $Sm_{0.987}Gd_{0.013}Al_2$ film. X-ray energy is 7.315 keV. The L_2Sm signal has been multiplied by -1.

makes the complete magnetization reversal impossible. Such a high coercivity can be related to the occurrence of antiphase boundaries (section 2). As shown in [13], the coercivity value increases with the density of antiphase boundaries, which play an important role as pinning centers of the domain walls.

When increasing temperature, the coercivity tends to decrease but it exhibits a pronounced anomaly that is absent for the pure $SmAl_2$ films (figure 4). The divergence of the coercive field is related to the thermal dependence of magnetization, presented in figure 5(a) for the same film. The measurements have been performed in increasing temperature under zero external field, after a $+7$ T field cooling process from 300 to 10 K. The substitution of 1.3% of Sm atoms by Gd atoms does not modify the ordering temperature, close to 127 K. However, it induces a slight reduction of the magnetic moment over the entire temperature range and the occurrence of a

compensation temperature (108 K), where the magnetization drops to zero (figure 5(a)). The divergence of the coercive field at 108 K in the Gd-substituted film (figure 4) is related to this compensated state: in this temperature range where the magnetic moment becomes considerably small, the Zeeman contribution also becomes small. The magnetic field required for the magnetization reversal thus increases significantly and tends towards infinity for zero magnetization. Finally, it is noticeable that the magnetization changes sign at the compensation point and is negative above 108 K (figure 5(a)): this result will be explained in section 4.

The value of the coercive field at 12 K depends on the Gd content (figure 4: inset). It increases with Gd content for x smaller than approximately 3% and decreases for x larger than 4%. For intermediate values of x, it is larger than 7 T, the maximum field available in our set-up. This high value is again correlated to the compensation state that occurs at low temperature for $x = 3.5\%$.

Moreover, the value of the coercive field depends on the film thickness. It increases when the thickness decreases: for thicknesses smaller than 300 nm, the coercive field exceeds 7 T. A detailed study of the antiphase boundary evolution with the film thickness should explain this behavior.

A systematic study of several films with different Gd contents has shown that the compensation temperature decreases when the Gd content increases: it is reduced to 81 K for 2.3% and to 50 K for 3.2% (figure 6). A similar behavior has been observed in bulk compounds [2, 3, 5, 14, 15].

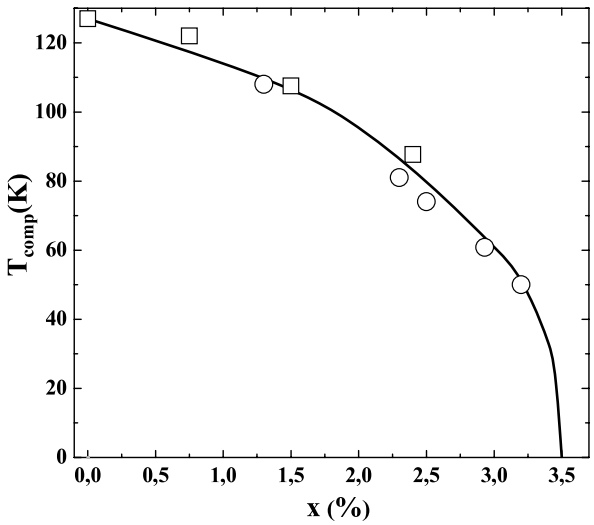

Figure 6. Compensation temperature versus the composition x for 265 nm thick (open circles) and 880 nm thick (open squares) $Sm_{1-x}Gd_xAl_2$ films.

4. Ferromagnetic order at the compensation point

In this paragraph, we focus on the 880 nm thick (111)$Sm_{0.987}Gd_{0.013}Al_2$ film. In order to investigate the magnetic state of the Sm and Gd at the compensation point, we have performed x-ray magnetic circular dichroism measurements at the $L_{2,3}$ edges of these atoms. XMCD experiments were carried out at the ID12 beam line of the European Synchrotron Radiation Facility (ESRF) in Grenoble (France) [16]. The sample was mounted on a cold finger of a constant-flow helium cryostat, which was inserted in a bore of a 6 T superconducting magnet. The magnetic field was applied along the [111] easy magnetization direction of the sample and set parallel to the incident x-ray beam. The XMCD spectra were obtained as a direct difference of x-ray absorption spectra recorded at Sm and Gd $L_{2,3}$ edges, in total fluorescence detection mode, with left and right circularly polarized x-rays. This approach keeps the direction of the magnetic field fixed and therefore allows one to measure element selective hysteresis loops and/or magnetization as a function of temperature. Both kinds of measurements are performed at a fixed energy, which corresponds to the maximum of the XMCD signal at the absorption edge of a given atom.

Typical XMCD spectra collected at the $L_{2,3}$ edges of Sm and Gd at 20 K are presented in figure 7. The dichroic signal at the Sm L_3 edge presents two features that could be assigned to dipolar ($2p \rightarrow 5d$) transitions and quadrupolar ($2p \rightarrow 4f$) transitions; the latter peak is located at -6 eV. The XMCD signal at the Sm L_2 edge exhibits only a single dispersive shape feature which could be assigned to dipolar transitions. On the other hand, the XMCD signals at the $L_{2,3}$ edges of Gd are fully dominated by dipolar contributions and we do not observe any feature that could be assigned to quadrupolar transitions. The signal-to-noise ratio is rather poor in the XMCD spectra recorded at the Gd L edges: this is due to the small amount of Gd in the sample and to the fact that the Gd absorption signal is superposed with a strong Sm signal. The shape of all the above XMCD spectra does not change with temperature (from the ordering temperature down to 20 K).

The XMCD spectra at $L_{2,3}$ edges are related via the sum rules derived by Carra *et al* [17] to the sign and magnitude of the spin and orbital moments of the probed band. In the case of rare earth elements the applicability of these sum rules is questionable because of (i) the presence of a quadrupolar transitions and (ii) the exchange interaction between the 4f electrons and the 5d spin-up and spin-down subbands [18]. Nevertheless, we can try to correlate the sign of the dichroic spectra to the 5d spin orientation, assuming that the orbital moment is much smaller. As shown by several experiments [7], for rare earths of the first half of the series a positive XMCD signal at the L_2 (respectively L_3) edge characterizes a parallel (antiparallel) coupling between 5d spin and applied field. For rare earths of the second half of the series, a positive XMCD signal at the L_2 (respectively L_3) edge characterizes an antiparallel (parallel) coupling between 5d spin and applied field.

Figures 5(b) and (c) present the variation with temperature of the XMCD signal measured at the Sm and Gd L_3 edges and at the Sm L_2 edge. The Gd signal has been multiplied by a factor of 6. The Sm signal at the L_2 edge has been multiplied by -1 because of the intrinsic opposite signs for signals measured at the L_3 and L_2 edges of rare earth metal. The data are collected in increasing temperature under zero magnetic field after a 6 T field cooling process. The results are compared with

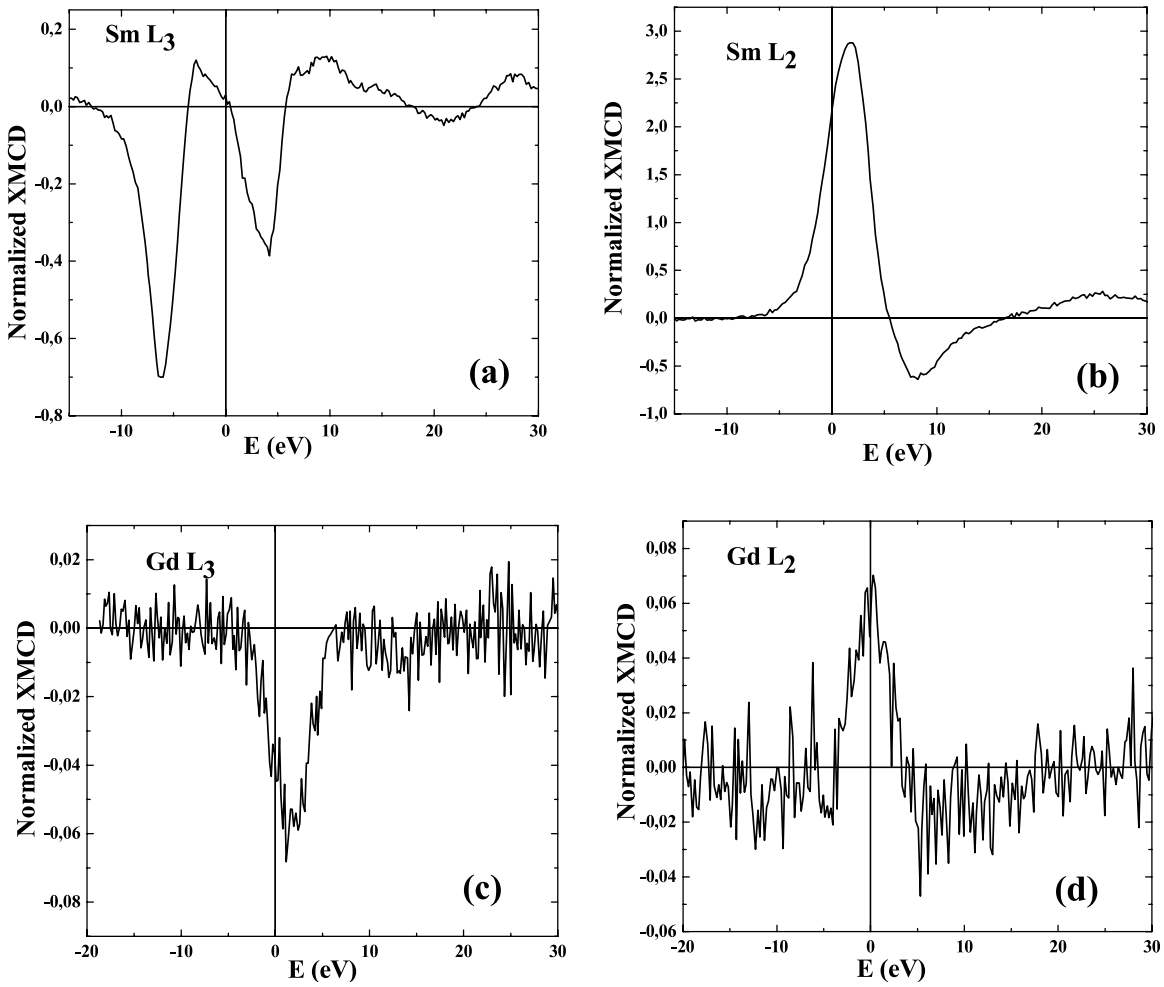

Figure 7. Normalized x-ray magnetic circular dichroic signal measured at 20 K and under 6 T at the Sm L_3 edge (a) and L_2 edge (b) and at the Gd L_3 edge (c) and L_2 edge (d) for the 880 nm thick $Sm_{0.987}Gd_{0.013}Al_2$ film. The signals are expressed as percentages of the jump at the edge.

the macroscopic magnetization curve (figure 5(a)). A number of conclusions can be drawn from these experiments.

(i) The Sm and Gd 5d spin moments are parallel to each other and exhibit very similar temperature variations.
(ii) The Sm and Gd 5d spin moments are antiparallel to the direction of applied field at 12 K.
(iii) The Sm and Gd 5d spin moments are obviously different from zero at the compensation temperature, a temperature where the total magnetization is zero (vertical line).

The first point is in total agreement with the expected coupling between Gd and Sm magnetic contributions. Magnetic interactions between rare earth metals are mediated by the positive coupling between spin contributions. The Gd spin contribution thus adds to the Sm one and contributes to the increase of the overall spin contribution [19].

The second conclusion reveals that the spin contribution to the total magnetic moment is not the dominant one at 12 K in zero field after a +6 T field cooling process. The orbital contribution due to the Sm atoms is the dominant one and aligns parallel to the field at low temperature. The important fact is that the total spin contribution becomes dominant above compensation. However, both contributions do not change sign over the entire temperature range since the field is zero. Thus, the XMCD data allow a better understanding of the two features of the macroscopic magnetic magnetization temperature dependence (figure 5(a)): while the 5d Sm spin keeps its orientation, the total moment changes sign at T_{comp} and is negative above 108 K. The compensation point is the result of the perfect cancelation between antiparallel orbital Sm contribution and spin (Sm + Gd) contributions.

The last observation is the direct proof that the long range ferromagnetic order for the (Sm + Gd) magnetic lattice is still present despite the zero magnetization. Due to the positive coupling between Sm and Gd spin moments, all the spins are orientated towards the field direction, in contrast to the case of compensated ferrimagnetic compounds. This result is in agreement with Compton diffraction [4] and XMCD [5] experiments performed on bulk compounds.

Figure 8 presents macroscopic magnetization and XMCD measurements performed under a zero applied field after two different magneto-thermal treatments. In both cases, the sample is cooled under zero field down to a temperature T_{mag}. A 6 T field is applied and then switched back to zero. The first measurement (empty squares) was made while cooling from 120 to 45 K, after applying 6 T at $T_{mag} = 114$ K $> T_{comp}$.

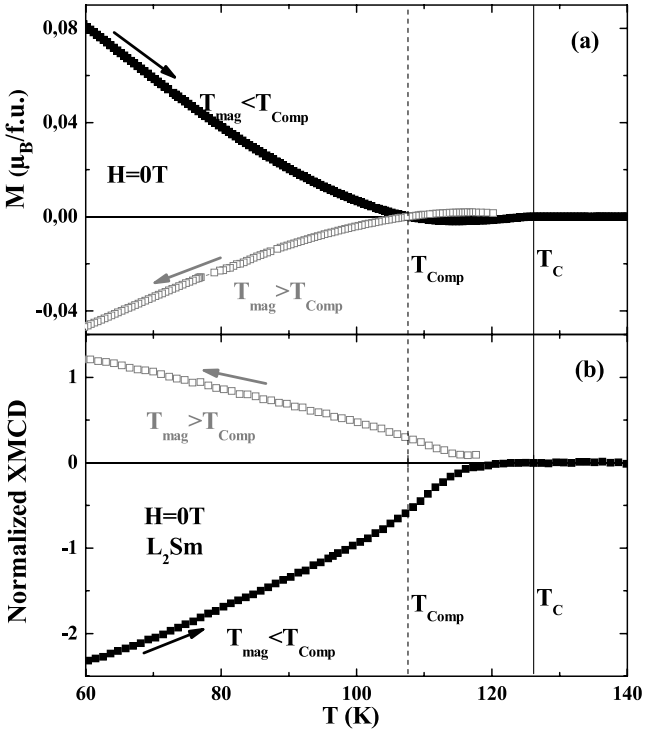

Figure 8. Temperature dependent magnetization (a) and XMCD signal at the L_2 Sm edge (b) measured under zero magnetic field after two magneto-thermal treatments: 6 T applied at a so-called magnetization temperature T_{mag} when $T_{mag} > T_{comp}$ (open squares) and $T_{mag} < T_{comp}$ (filled squares). The L_2Sm signal has been multiplied by -1.

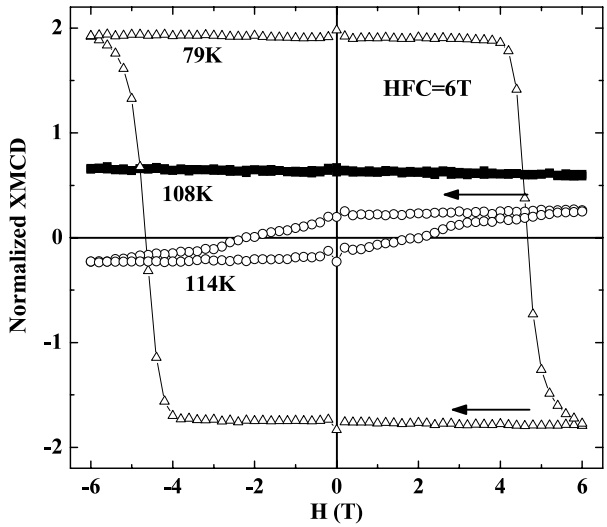

Figure 9. Sm L_2 edge hysteresis loops realized after field cooling under 6 T at 79 K (open triangles), 108 K (filled squares) and 114 K (open circles).

The second measurement (filled squares) was made while heating from 45 to 150 K, after applying 6 T at $T_{mag} = 45$ K $< T_{comp}$. For both magneto-thermal treatments, the magnetization is opposite in the whole temperature range. In both cases, it changes sign at T_{comp} (figure 8(a)). When the field is applied below (respectively above) T_{comp}, the XMCD signal at the Sm L_2 edge is negative (respectively positive), which is the signature of Sm 5d spin moment aligned antiparallel (respectively parallel) to the field for the whole temperature range (figure 8(b)). These experimental results confirm again that the total orbital moment dominates below T_{comp}, while the total spin moment dominates above T_{comp}.

It is to be underlined that the amplitudes of the dichroic signal and of the macroscopic magnetization measured after the first magneto-thermal treatment (empty squares) are smaller. This observation can be correlated to a less efficient Zeeman contribution close to the compensation temperature. However, additional experiments are necessary to resolve the magnetic configuration (tilt of the moments, perpendicular magnetization domains ...) associated with this lower spin moment state.

The important result is that the orientation of the spin moments at the compensation temperature can be controlled by choosing the magnetization temperature. The sign of the spin moment depends on the dominant magnetic contribution (spin or orbital one) at the magnetization temperature. The amplitude of the spin moment depends on the magnetization temperature. Its sign remains constant in the whole temperature range, since no magnetic field is applied.

In order to illustrate the ferromagnetic character of the film without magnetization, selective hysteresis loops at the Sm L_2 edge have been measured for three temperatures: below and above T_{comp} and at T_{comp} (figure 9). At 79 K, after a field cooled process, the XMCD signal is negative: the 5d moment is antiparallel to the applied field. At 114 and 108 K, the XMCD signal is positive: the 5d moments are parallel to the field. The XMCD loops measured at 79 and 114 K are characteristic of the 5d spin moment reversal. At the compensation temperature, the XMCD loop is flat, since the magnetic configuration in the film is not sensitive to the occurrence of the applied magnetic field. It is not possible to reverse the spin moments.

5. Conclusion

We have shown that it is possible to grow high quality single crystalline (111)$Sm_{1-x}Gd_xAl_2$ films that are zero magnetization ferromagnets at the compensation temperature. The compensation temperature depends on the Gd content and is close to the value measured in bulk compounds. The single crystalline $Sm_{1-x}Gd_xAl_2$ films exhibit a magnetization direction perpendicular to the growth plane and a huge coercive field that diverges at the compensation temperature. Using x-ray magnetic circular dichroism at Sm and Gd $L_{2,3}$ edges, we have directly evidenced the occurrence of a long range spin polarization of the Sm and Gd 5d conduction electron spin at T_{comp}, and a parallel coupling between total spin moment of Sm^{3+} and Gd^{3+}. Moreover, the spin orientation can be tailored: it depends on the magnetic history of the sample.

The next step is to integrate this new material in more complex magnetic heterostructures.

(i) To get a better understanding of this material's fundamental properties, especially concerning its transport properties as a potential spin polarizer for an electric current

(this includes measuring spin polarization using a superconducting contact point [20]).

(ii) To take advantage of its unusual zero magnetization ferromagnetic order to address specific issues concerning for example magnetic coupling or exchange bias phenomena.

Another aspect is to develop new original zero moment ferromagnets, with higher Curie temperature and extended compensation state.

References

[1] Adachi H, Ino H and Miwa H 1999 *Phys. Rev.* B **59** 11445
[2] Adachi H and Ino H 1999 *Nature* **401** 148
[3] Taylor J W, Duffy J A, Bebb A M, Lees M R, Bouchenoire L, Brown S D and Cooper M J 2002 *Phys. Rev.* B **66** 161319
[4] Adachi H, Kawata H, Hashimoto H, Sato Y, Matsumoto I and Tanaka Y 2001 *Phys. Rev. Lett.* **87** 127202
[5] Qiao S, Kimura A, Adachi H, Iori K, Miyamoto K, Xie T, Namatame H, Taniguchi M, Tanaka A, Muro T, Imada S and Suga S 2004 *Phys. Rev.* B **70** 134418
[6] Qiao S, Kimura A, Adachi H, Kame T, Yoshikawa K, Yaji K, Sato H, Takeda Y, Namatame H, Taniguchi M, Tanaka A, Muro T, Imada S and Suga S 2004 *Physica* B **351** 333
[7] Buschow K 1979 *Rep. Prog. Phys.* **42** 1374
[8] Oderno V, Dufour C, Dumesnil K, Mangin P and Marchal G 1996 *J. Cryst. Growth* **165** 175
[9] Avisou A, Dufour C, Dumesnil K and Pierre D 2006 *J. Cryst. Growth* **297** 239
[10] Buschow K, van Diepen A and de Wijn H 1973 *Phys. Rev.* B **8** 5134
[11] Dufour C, Avisou A and Dumesnil K 2008 *J. Appl. Phys.* **103** 07E135
[12] Mougin A, Dufour C, Dumesnil K and Mangin P 2000 *Phys. Rev.* B **62** 9517
[13] Bollero A, Ziese M, Höhne R, Semmelhack H C, Köhler U, Setzer A and Esquinazi P 2005 *J. Magn. Magn. Mater.* **285** 279
[14] Barla A, Sanchez J P, Givord F, Boucherle J X, Doyle B P and Rüffer R 2005 *Phys. Rev.* B **71** 012407
[15] Chen X H, Wang K Q, Hor P H, Xue Y Y and Chu C W 2005 *Phys. Rev.* B **72** 054436
[16] Rogalev A, Goulon J, Goulon-Ginet C and Malgrange C 2001 *Magnetism and Synchrotron Radiation* (*Springer Lecture Notes in Physics* vol 565) ed E Beaurepaire, F Scheurer, G Krill and J-P Kappler (Berlin: Springer) p 60
[17] Carra P, Thole T, Altarelli M and Wang X 1993 *Phys. Rev. Lett.* **70** 694
[18] Ankudinov A L, Rehr J J, Wende H, Scherz A and Baerschke K 2004 *Europhys. Lett.* **66** 441
[19] Grover A K, Malik S K, Vijayaraghavan R and Shimizu K 1979 *J. Appl. Phys.* **50** 7501
[20] Soulen R J, Bryers J M, Orsofsky M S, Nadgorny B, Ambrose T, Cheng S F, Broussard J P, Tanaka C T, Nowak J, Moodera J S, Barry A and Coey J M D 1998 *Science* **282** 85